Biogeosciences, 12, 209–221, 2015
www.biogeosciences.net/12/209/2015/
doi:10.5194/bg-12-209-2015

Biogeosciences Open Access

Variable C : N : P stoichiometry of dissolved organic matter cycling in the Community Earth System Model

R. T. Letscher, J. K. Moore, Y.-C. Teng, and F. Primeau

Earth System Science, University of California, Irvine, CA, USA

Correspondence to: R. T. Letscher (robert.letscher@uci.edu)

Received: 22 April 2014 – Published in Biogeosciences Discuss.: 16 June 2014
Revised: 22 October 2014 – Accepted: 1 December 2014 – Published: 12 January 2015

Abstract. Dissolved organic matter (DOM) plays an important role in the ocean's biological carbon pump by providing an advective/mixing pathway for $\sim 20\,\%$ of export production. DOM is known to have a stoichiometry depleted in nitrogen (N) and phosphorus (P) compared to the particulate organic matter pool, a fact that is often omitted from biogeochemical ocean general circulation models. However the variable C : N : P stoichiometry of DOM becomes important when quantifying carbon export from the upper ocean and linking the nutrient cycles of N and P with that of carbon. Here we utilize recent advances in DOM observational data coverage and offline tracer-modeling techniques to objectively constrain the variable production and remineralization rates of the DOM C : N : P pools in a simple biogeochemical-ocean model of DOM cycling. The optimized DOM cycling parameters are then incorporated within the Biogeochemical Elemental Cycling (BEC) component of the Community Earth System Model (CESM) and validated against the compilation of marine DOM observations. The optimized BEC simulation including variable DOM C : N : P cycling was found to better reproduce the observed DOM spatial gradients than simulations that used the canonical Redfield ratio. Global annual average export of dissolved organic C, N, and P below 100 m was found to be $2.28\,\mathrm{Pg\,C\,yr^{-1}}$ ($143\,\mathrm{Tmol\,C\,yr^{-1}}$), $16.4\,\mathrm{Tmol\,N\,yr^{-1}}$, and $1\,\mathrm{Tmol\,P\,yr^{-1}}$, respectively, with an average export C : N : P stoichiometry of 225 : 19 : 1 for the semilabile (degradable) DOM pool. Dissolved organic carbon (DOC) export contributed $\sim 25\,\%$ of the combined organic C export to depths greater than 100 m.

1 Introduction

Dissolved organic matter (DOM) is an important pool linking nutrient cycles of nitrogen (N) and phosphorus (P) to the ocean's carbon cycle. Following its net production in the surface ocean, DOM provides an advective pathway for removal of biologically fixed carbon (C) to the deep ocean, accounting for $\sim 20\,\%$ of the C exported within the ocean's biological pump (Hansell, 2013). Remineralization of DOM in the ocean's interior is carried out by microbial heterotrophs, respiring C while releasing inorganic N and P nutrients back into the water column. The concept of the Redfield ratio (Redfield, 1958; Redfield et al., 1963) has been a unifying paradigm in ocean biogeochemistry linking the stoichiometry of biological production and phytoplankton cellular material to that of the remineralization of detrital organic matter (OM) and inorganic nutrient ratios in the water column. At the global scale, production/decomposition of particulate OM (POM) in the ocean is thought to largely follow the canonical Redfield ratio of 106 : 16 : 1 for C : N : P, however some recent studies have suggested more variable C : N : P ratios (i.e., Martiny et al., 2013a, b) and only recently has variable C : N : P stoichiometry been introduced into Earth system models (e.g., Vichi et al., 2007; Dunne et al., 2013). Large deviations from the Redfield ratio have been documented for DOM (Aminot and Kérouel, 2004; Hopkinson and Vallino, 2005). Hopkinson and Vallino (2005) found DOM production and decomposition to follow a stoichiometry of 199 : 20 : 1, indicating the more efficient export of C within DOM per mole of N and P relative to sinking POM. This finding is significant in light of evidence that future perturbations to the ocean from global climate change may favor enhanced partitioning of production to DOM (Wohlers et al., 2009; Kim et al., 2011). Thus accounting for variable

stoichiometry within the DOM pool that deviates from the Redfield ratio requires a re-evaluation of the controls on C export and their response to future perturbations due to climate change.

Here we aim to utilize recent advances in DOM data coverage to incorporate variable production and decomposition stoichiometry within the DOM tracers of the Biogeochemical Elemental Cycling (BEC) model in order to improve representation of this important carbon export flux and associated nutrient cycles. The BEC tracks the cycling of key biogeochemical tracers (e.g., C, N, P and Fe) and runs within the ocean general circulation component of the Community Earth System Model (CESM) (Moore et al., 2004). The current release of CESM v1.2.1 contains five DOM-related tracers: semilabile DOC (dissolved organic carbon), DON (dissolved organic nitrogen), and DOP (dissolved organic phosphorous) pools as well as refractory DON and DOP pools (Moore et al., 2014). Here we have added a sixth DOM tracer, refractory DOC. Our approach is to optimize the BEC DOM parameters using available observations, by applying a fast offline solver based on a direct-matrix inversion (DMI) of a linear model of DOM cycling; an approach similar to previous applications for marine radiocarbon (Khatiwala et al., 2005) and marine organic matter cycling (Kwon and Primeau, 2006; Hansell et al., 2009). The 3-D ocean circulation is obtained from the offline tracer-transport model for the ocean component of the CESM (Bardin et al., 2014). The DMI solver uses a parallel multifrontal sparse matrix inversion approach as implemented in the MUMPS (MUltifrontal Massively Parallel Sparse direct Solver) (Amestoy et al., 2001, 2006) to quickly obtain the equilibrium solutions needed to objectively calibrate the biogeochemical parameters of the DOM cycling model by minimizing the misfit between the model and observations. The DOM cycling parameters from the equilibrium solution of the offline model are then incorporated within the BEC and optimized with only minor additional tuning.

The remainder of this article is organized as follows. Section 2 describes (1) the current representation of DOM cycling in the BEC v1.2.1, (2) the global ocean data set of DOM observations utilized for the optimization, (3) the structure of the offline DOM cycling model and the DMI solver, and (4) the modified BEC model with improved DOM cycling parameters with the metrics employed for optimization. Section 3 details the results of (1) the offline DOM cycling model solution, (2) the reference CESM BEC v1.2.1 simulation, as well as (3) the BEC simulation with optimized DOM cycling, including a comparison of DOM cycling metrics. Sections 3.4 and 3.5 describe a comparison of multiple DOM cycling schema and an evaluation of direct uptake of DOP by phytoplankton in the BEC model, respectively. We conclude with a discussion and summary of our results in Sect. 4.

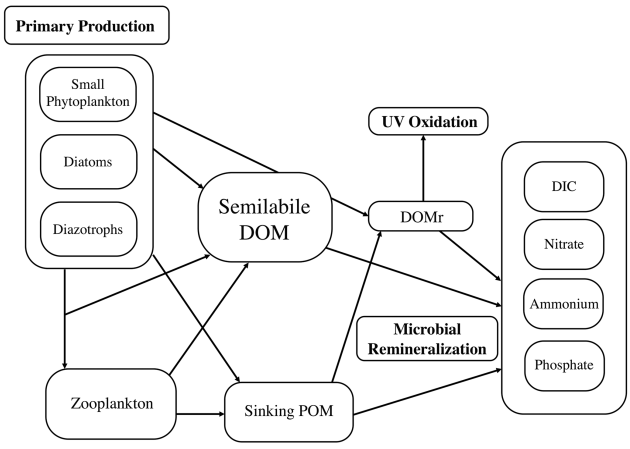

Figure 1. Schematic of organic matter cycling in the CESM BEC. Primary production is carried out by three phytoplankton functional types: small phytoplankton (which also contains a subgroup of calcifying phytoplankton), diatoms, and diazotrophs. Sources to DOM include direct losses from phytoplankton/zooplankton and from zooplankton grazing of phytoplankton. The major sink for DOM is microbial remineralization, parameterized with an assigned lifetime which differs between the euphotic zone and the mesopelagic ocean. A small fraction of phytoplankton production is converted to refractory DOM in the upper ocean with an additional source to DOMr from degradation of sinking POM in the mesopelagic. DOMr is also lost via UV photo-oxidation in the surface layer (< 10 m). The products of organic matter remineralization are dissolved inorganic carbon, nitrate, ammonium, and phosphate.

2 Methods

2.1 DOM cycling in the standard BEC v1.2.1

Model simulations with the optimized DOM parameters are compared against a reference simulation using the standard version of the CESM BEC v1.2.1, which we refer to as REF. The BEC model runs within the ocean physics component of CESM1 (Gent et al., 2011), which is the Parallel Ocean Program v2 (POP2; Smith et al., 2010). Detailed description and evaluation of the ocean general circulation model is given by Danabasoglu et al. (2011). Additional documentation, model output, and model source code are available online (www2.cesm.ucar.edu). The REF simulation has a nominal horizontal resolution of 1° with 60 vertical levels ranging in thickness from 10 m (in the upper 150 m) with increasing layer thickness increasing with depth below 150 m. Results are presented for the final 20 yr annual average from a 310 yr simulation.

A flowchart of organic matter cycling in the BEC is shown in Fig. 1 and a list of DOM parameter values from REF are given in Table 1. Primary production is carried out amongst three phytoplankton groups, which take up available inorganic nutrients and have losses to zooplankton grazing, sinking POM, and semilabile DOM. Organic matter is

Table 1. Optimized DOM parameters from the DMI-enabled linear DOM model (DMI-DOM solver) and the modified DMI model (MOD DMI-DOM solver) as well as the REF and DOM OPT simulations of the CESM BEC. Euphotic zone: 0–100 m for the DMI-DOM models and depths where PAR > 1 % for REF and DOM OPT. The "flux to DOM" represents the fraction of PP that accumulates as DOM while the "fraction of DOM flux" represents the portion of the DOM production flux that accumulates as semilabile (SL) or refractory (R) DOM. Parameters $f_i|i = 1\cdots2, \kappa_i|i = 1\cdots4$ are defined in Eqs. (1)–(4). Surf: surface layer (< 10 m), reminR: remineralization rate, sp: small phytoplankton, diat: diatoms, diaz: diazotrophs, k: half saturation constant for DOP uptake, and NA: not applicable.

Parameter	DMI-DOM solver	MOD DMI-DOM solver	Parameter	REF	DOM OPT
	Flux to DOM (f_1)	Fraction of DOMprod flux	Flux to DOM		
			f_PP_doc	0.15	0.06
SLDOC	0.099	0.99	f_PP_don	0.15	0.04
SLDON	0.01	0.9885	f_PP_dop	0.15	0.06
SLDOP	0.095	0.997	parm_labile_ratio	0.85	0.94
			DOCrefract	NA	0.01
	(f_2)		DONrefract	0.08	0.0115
DOCr	0.006	0.01	DOPrefract	0.03	0.003
DONr	0.004	0.0115	f_to_don	NA	0.66
DOPr	0.0015	0.003			
			DOP uptake		
			sp_kDOP	0.26	0.25
DOP uptake	NA	NA	diat_kDOP	0.9	1.0
			diaz_kDOP	0.09	0.08
DOM lifetimes			DOM lifetimes		
– Euphotic zone			– Euphotic zone		
SLDOC: $1/\kappa_1$	34 yr	15 yr	DOC_reminR	250 d	15 yr
SLDON: $1/\kappa_1$	8.7 yr	15 yr	DON_reminR	160 d	15 yr
SLDOP: $1/\kappa_1$	5.8 yr	62 yr	DOP_reminR	160 d	60 yr
– Layer 1 (> −10 m)			– Layer 1 (> −10 m)		
RDOC: $1/\kappa_4$	NA	15 yr	DOCr_reminR	NA	20 yr
RDON: $1/\kappa_4$	NA	15 yr	DONr_reminR	2.5 yr	20 yr
RDOP: $1/\kappa_4$	NA	15 yr	DOPr_reminR	2.5 yr	20 yr
– Mesopelagic zone			– Mesopelagic zone		
SLDOC: $1/\kappa_2$	2.9 yr	5 yr	DOC_reminR	10 yr	5.5 yr
SLDON: $1/\kappa_2$	1.7 yr	5 yr	DON_reminR	4.4 yr	5 yr
SLDOP: $1/\kappa_2$	0.8 yr	4.5 yr	DOP_reminR	8.8 yr	4 yr
– Layer 2 : 60 (< −10 m)			– Layer 2 : 60 (< −10 m)		
RDOC: $1/\kappa_3$	20 000 yr	15 000 yr	DOCr_reminR	NA	16 000 yr
RDON: $1/\kappa_3$	9000 yr	8000 yr	DONr_reminR	670 yr	9000 yr
RDOP: $1/\kappa_3$	5000 yr	6000 yr	DOPr_reminR	460 yr	5000 yr

produced with a C : N : P stoichiometry set to the slightly modified Redfield ratio of Anderson and Sarmiento (1994), 117 : 16 : 1. Additional sources to semilabile DOM include grazing losses when phytoplankton are grazed by zooplankton as well as direct zooplankton losses. A variable fraction of DOM production is sent to the refractory DOM (DOMr) pool, with different fractions going to the dissolved organic N and P pools. Approximately 15 % of modeled primary production (PP) is sent to the DOM pool via these sources, with the remainder of PP cycling as POM. It is important to note that the BEC does not specifically track the total production/decomposition of DOM, which is estimated to be 30–50 % of net primary production (NPP) (Carlson, 2002; and references therein). Rather, BEC semilabile and refractory DOM tracers track the *accumulated* DOM pools that arise from the decoupling of DOM production and consumption in time and space and are thus subject to advection by the ocean circulation. These recalcitrant DOM fractions cycle on timescales of years to centuries and represent a smaller portion of NPP, i.e., ∼ 5–10 % (Hansell, 2013). The labile DOM pool, which cycles on timescales of minutes to days (Hansell, 2013) is not explicitly modeled and is instead rapidly converted to inorganic carbon and nutrients at each time step.

Microbial remineralization is the dominant sink for both POM and DOM pools and is parameterized by assigned remineralization rates. POM is remineralized following a prescribed remineralization vs. depth curve, with a length scale that increases with depth (Moore et al., 2014). Semilabile DOM pools are assigned lifetimes (1 / remineralization rate) that depend on the light field with model grid cells where

photosynthetically active radiation (PAR) is > 1 % of surface irradiance being assigned a euphotic zone lifetime. Semilabile DOM in model grid cells with PAR < 1 % is assigned a mesopelagic zone lifetime. Remineralization is more rapid for semilabile DOM in the euphotic zone, with lifetimes on the order of 5 months for DON + DOP and ∼ 8 months for DOC. Longer lifetimes for semilabile DOM are assigned in the mesopelagic zone with the order of remineralization lifetimes following C > P > N. Remineralization of refractory DOM follows a similar light dependence with a faster remineralization rate given to DOMr in euphotic zone grid cells to parameterize a sink via UV oxidation (Carlson, 2002). DOMr below the euphotic zone is remineralized over centennial timescales.

2.2 Database of DOM ocean observations

We compiled publicly available and literature observations of DOM concentrations into a single database for use in both the DMI-enabled linear DOM model as well as to evaluate our BEC DOM optimization model runs. Briefly, the database contains over 34 000 observations of DOC, > 18 000 observations of DON, and > 2000 observations of DOP. Geographic coverage for the five ocean basins is moderately balanced for observations of DOC and DON; however, the Atlantic Ocean dominates available DOP observations with DOP data completely lacking for the Indian, Southern, and Arctic oceans. Semilabile DOM is defined as the total observed DOM concentration less the refractory concentration as determined from the asymptotic concentration of DOM depth profiles. Refractory DOC concentrations vary by ocean basin in the range of 37.7 (South Pacific)–45.0 µM (Arctic). Globally constant concentrations are used for refractory DON (1.8 µM) and refractory DOP (0.03 µM). Full details of this DOM database are given elsewhere (Letscher and Moore, 2014).

2.3 Application of the DMI-enabled solver with a linear DOM cycling model

2.3.1 First iteration – DOM source from BEC PP

The linear DOM cycling model cycles DOM with one source/sink and uses an idealized annual ocean circulation in offline mode from the CESM POP2 ocean circulation model (Bardin et al., 2014); nominal $1^\circ \times 1^\circ$ horizontal resolution with 60 vertical levels, i.e., the same grid as the standard BEC v1.2.1. In this simple model of DOM cycling, two tracers of DOM are simulated for each element, C, N, and P: semilabile (SLDOM) and refractory (RDOM). The source for each DOM tracer is parameterized as some variable fraction, f, of primary production and is formed within the top model grid level with a thickness of 10 m. The sink for each DOM fraction is microbial remineralization parameterized with an assigned remineralization rate, κ, that differs for the euphotic zone and deep ocean layers in the case of SLDOM. The conservation equations for each DOM tracer are

$$\frac{\partial}{\partial t}\mathrm{SLDOM} + \mathbf{T}\mathrm{SLDOM} = f_1\mathrm{PP} - \begin{cases} \kappa_1\mathrm{SLDOM} \\ \text{if } z > -100\,\mathrm{m} \\ \kappa_2\mathrm{SLDOM} \\ \text{if } z < -100\,\mathrm{m} \end{cases}, \quad (1)$$

$$\frac{\partial}{\partial t}\mathrm{RDOM} + \mathbf{T}\mathrm{RDOM} = f_2\mathrm{PP} - \kappa_3\mathrm{RDOM}\,, \quad (2)$$

where **T** is the advection–diffusion transport operator (a sparse matrix constructed using output from the dynamical CESM POP2 model as described in Bardin et al., 2014) and PP is the annual average 3-D primary production field from the coupled ocean–atmosphere run of the CESM for the 1990s (Moore et al., 2013).

We tested the sensitivity of the linear DOM model results to multiple production functions (CESM PP, DOM production flux from the BEC, satellite estimated PP); however, results suggest the differing source functions do not appreciably alter modeled DOM distributions or parameter values.

Our initial construction of the linear DOM model allowed the sum of $f_1 + f_2$ to vary continuously between 0 and 0.5 and $\kappa_i | i = 1 \cdots 3$ to vary logarithmically between 0.25 and 20 000 yr^{-1} by 24 discrete values. The direct-solver technique makes it possible to objectively calibrate these parameters, $f_i\kappa_i | i = 1 \cdots 3\{f_1, f_2, \kappa_1, \kappa_2, \kappa_3\}$, by using a numerical optimization algorithm that rapidly tests each permutation of the discretized κi values, scaled by f_i, in order to find the parameter set that minimizes the root mean square difference in the misfit between the model-predicted and observed DOM concentration. A separate linear DOM model (Eqs. 1, 2) is solved for the DOC, DON, and DOP cases. The DMI solver allows us to determine very efficiently the optimal lifetimes for the various DOM pools. It is not practical to determine these using multiple forward simulations of the full CESM BEC, which would require years to decades of computer time.

2.3.2 Optimized DOM parameter incorporation into the BEC model

The optimized parameter values obtained from the DMI-enabled linear DOM model were incorporated within the BEC to improve its representation of DOM cycling. The BEC model has two tracers for each DOM pool, semilabile and refractory, with differing lifetimes for the euphotic vs. mesopelagic zones. Thus the SLDOM lifetimes, κ_1 and κ_2, from the DMI-enabled DOM model were applied to the BEC model semilabile tracers for the euphotic zone and mesopelagic, respectively. The RDOM lifetime from the DMI-enabled DOM model was applied throughout the full water column of the BEC model. Further fine-tuning of DOM lifetimes was carried out to provide the best DOM optimized case, using the mean bias of the modeled concentrations versus the observations and the

log-transformed regression correlation coefficient between simulated and observed DOM in the upper ocean, 0–500 m, as comparison metrics. The BEC simulation containing the set of improved DOM cycling parameters following the first iteration of the DMI-enabled linear DOM model is termed DOM DEV.

2.3.3 Second iteration of DMI-enabled linear DOM model – DOM source from BEC DOM production flux

Initial improvements to DOM cycling metrics within the BEC model were large upon incorporation of the DMI-enabled linear DOM model parameter values; however, because of differences between the offline model and the full BEC model, further improvements to the DOM tracer lifetimes were possible. To achieve this the DMI-enabled linear DOM model was modified such that the production for each tracer was held constant allowing only the remineralization rate, κ_i, to be optimized from a choice of 48 discrete tracer lifetimes spanning the range 0.7–20 000 yr^{-1}. Rather than using PP to get the production flux of each DOM tracer, the semilabile and refractory DOM production fluxes (SLDOMprod, RDOMprod) were extracted from the DOM DEV simulation and prescribed in the modified DMI-enabled DOM model. The fraction of SLDOMprod and RDOMprod to be applied each $\kappa_i | i = 1 \cdots 4$ was diagnosed from the relative proportions of each tracer residing in the euphotic or deep layers at the end of the DOM DEV simulation of the BEC (see Fig. 2). At this step it was also desired to solve for the remineralization rate associated for a secondary sink for DOMr due to photo-oxidation in the surface layer. Thus Eqs. (1) and (2) were modified to become Eqs. (3) and (4) as follows:

$$\frac{\partial}{\partial t}\mathrm{SLDOM} + \mathbf{T}\mathrm{SLDOM} = \mathrm{SLDOMprod} - \begin{cases} \kappa_1 \mathrm{SLDOM} & \text{if } z > -100\,\mathrm{m} \\ \kappa_2 \mathrm{SLDOM} & \text{if } z < -100\,\mathrm{m} \end{cases}, \quad (3)$$

$$\frac{\partial}{\partial t}\mathrm{RDOM} + \mathbf{T}\mathrm{RDOM} = \mathrm{RDOMprod} - \begin{cases} \kappa_4 \mathrm{RDOM} & \text{if } z > -10\,\mathrm{m} \\ \kappa_3 \mathrm{RDOM} & \text{if } z < -10\,\mathrm{m} \end{cases}. \quad (4)$$

The results obtained from the modified DMI-enabled linear DOM model were incorporated into the final DOM optimized (DOM OPT) simulation of the BEC following minor tuning of the κ parameter values.

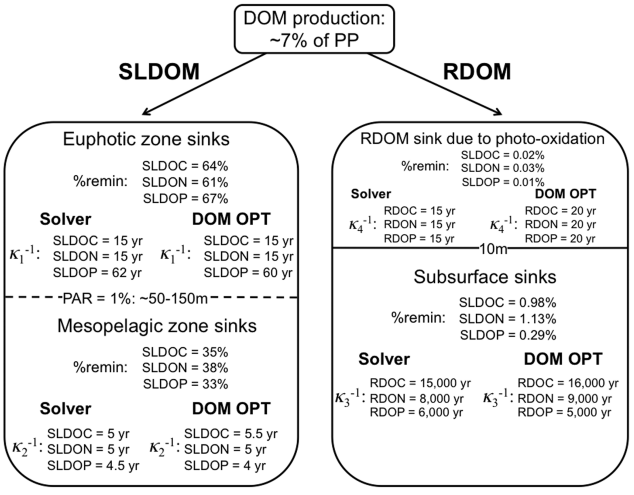

Figure 2. Configuration of the DOM remineralization scheme and parameter values from the modified DMI-enabled DOM model (solver) and the DOM OPT simulation of the CESM BEC. Note the only minor changes to tracer lifetimes, κ_i^{-1}, between the modified DMI-DOM model and the DOM OPT simulation. The value "%remin" represents the percentage of the DOM production flux that is remineralized within each depth horizon on an annual basis and is common to both models.

3 Results

3.1 DOM parameter output from the DMI-enabled linear DOM model

3.1.1 First iteration – DOM source from BEC PP

The objectively optimized DOM parameter values from the solutions to the DMI-enabled linear DOM model (DMI-DOM solver) are shown in Table 1. The fraction of the PP flux that accumulates as DOC, DON, and DOP is $\sim 10\,\%$, with the percentage cycling as refractory DOM: DOCr = 0.6 %, DONr = 0.4 %, and DOPr = 0.15 %. Optimized semilabile DOC exhibited the longest lifetimes with a lifetime of 34 yr in the euphotic zone (EZ) and 2.9 yr in the mesopelagic zone (MZ). Semilabile DON had an intermediate lifetime with respect to DOC and DOP, with an EZ lifetime of 8.7 yr and MZ lifetime of 1.7 yr. Semilabile DOP had the shortest lifetimes, with an EZ lifetime of 5.8 yr and MZ lifetime of 0.8 yr. Optimization of the parameters for the refractory pools yielded lifetimes of 20 000, 9000, and 5000 yr for DOCr, DONr, and DOPr, respectively.

3.1.2 Second iteration of DMI-enabled linear DOM model – DOM source from BEC DOM production flux

Results from the modified DMI-enabled linear DOM model (MOD DMI-DOM solver), which used the BEC DOM production flux from the DOM DEV simulation are shown in

Table 2. DOM production, export, and stoichiometry metrics for the REF and DOM OPT simulations against observational constraints.

Metric	REF	DOM OPT	H09[a]	Metric	REF	DOM OPT	OBS[b]
DOM export 100 m	Tmol (Pg) yr^{-1}	Tmol (Pg) yr^{-1}	Pg yr^{-1}	DOM stoichiometry 100 m			
DOC prod	874 (10.5)	346 (4.16)	3.7	Total pools			
DOC remin	731 (8.78)	157 (1.88)	1.8	C : N	–	15.9	14.0
DOC export	143 (1.72)	189 (2.28)	1.9	N : P	19.4	29.4	40.6
				C : P	–	468.7	580.8
DON prod	120	30.7	–				
DON remin	95.0	14.3	–	Semilabile pools			
DON export	25.0	16.4	–	C : N	7.3	11.9	7.5
				N : P	16.4	18.8	32.2
DOP prod	7.43	2.94	–	C : P	119	223.5	272.7
DOP remin	6.13	1.96	–				
DOP export	1.30	0.98	–				

[a] Hansell et al. (2009) result from a DOC data assimilative biogeochemical/circulation model.
[b] Letscher and Moore (2014) result from analysis of marine DOM database.

Fig. 2 and Table 1. Approximately 7 % of PP is routed to production of DOM, which is divided amongst semilabile (SLDOM) and refractory pools (RDOM). Remineralization lifetimes (κ_i^{-1}) differ for SLDOM depending on location in the water column with longer lifetimes for the euphotic zone (depths where PAR > 1 %) than for the mesopelagic zone. A faster rate of RDOM remineralization is assigned in the surface layer (< 10 m) to parameterize a sink due to photo-oxidation. The parameter, %remin, represents the percentage of the DOM production flux that is remineralized within each depth horizon on an annual basis with the sum equal to 100 % and is diagnosed from the DOM DEV simulation. The relative magnitude of SLDOM remineralization that occurs within the EZ vs. the MZ was found to be $\sim 1.8 : 1$ (Fig. 2). Only a small percentage of RDOM remineralization occurs in the surface layer, i.e., 0.01–0.03 % (Fig. 2). The optimal tracer lifetimes from the modified DMI-DOM model were 15 yr for SLDOC in the EZ, 5 yr for SLDOC in MZ, 15 000 yr for RDOC, and 15 yr for RDOC whilst in the surface layer (< 10 m). DON tracer lifetimes were: 15 yr for EZ SLDON, 5 yr for MZ SLDON, 8000 yr for RDON, and 15 yr for RDON at the surface. DOP tracer lifetimes were 62 yr for SLDOP in the EZ, 4.5 yr for MZ SLDOP, 6000 yr for RDOP, and 15 yr for photo-oxidation removal.

3.2 Modeled DOM in the standard CESM BEC v1.2.1 (REF simulation)

A set of metrics were used to assess the performance and improvements to DOM cycling for the CESM BEC simulations including the global integrals of DOM production, export, and C : N : P stoichiometry (Table 2) as well as the mean bias and correlation coefficient (r) of the simulated DOM concentrations against the observational data set in the upper 500 m (Table 3). Results and comparison of DOM cycling metrics from the REF simulation are presented in Tables 2 and 3.

Table 3. DOM mean bias and correlation coefficient in relation to the DOM observations within the upper ocean (0–500 m depth) for the REF and DOM OPT 1° simulations. Observations of semilabile DOM are calculated as the total observed DOM concentration less the asymptotic concentration below 1000 m in each ocean basin.

Metric	REF		DOM OPT	
Total DOM 0–500 m	mean bias	log r	mean bias	log r
DOC	NA	NA	+4 %	0.834
DON	+16 %	0.626	+2 %	0.663
DOP	+32 %	0.362	+7 %	0.439
Semilabile DOM 0–500 m				
DOC	+24 %	0.734	+46 %	0.810
DON	−20 %	0.632	+7 %	0.658
DOP	+4 %	0.388	+4 %	0.431

DOC. Total DOC production in the euphotic zone (upper 100 m) for the REF simulation is 10.5 Pg C yr^{-1} (Table 2). About 85 % of this DOC production is remineralized within the euphotic zone, yielding DOC export from the euphotic zone of ~ 1.7 Pg C yr^{-1}. Modeled semilabile DOC concentrations from the REF simulation are shown for the surface (Fig. 3a) with observations overlain by the colored dots. The spatial extent of regions with elevated (> 30 µM) semilabile DOC concentrations (i.e., the subtropical gyres) is too large in the REF simulation compared to observations. Large overestimates of simulated DOC are found in the Southern Ocean. Modeled semilabile DOC concentrations for the REF simulation at 200 m are shown in Fig. 3b. Model underestimates (up to ∼ 75 %) are observed in the oxygen-deficient zones in the eastern basins of the equatorial regions. Note that CESM v1.2.1 lacks a DOCr tracer so that simulated DOC is for the semilabile pool only (here we have subtracted the observed deep ocean DOC concentration for each basin from the DOC observations).

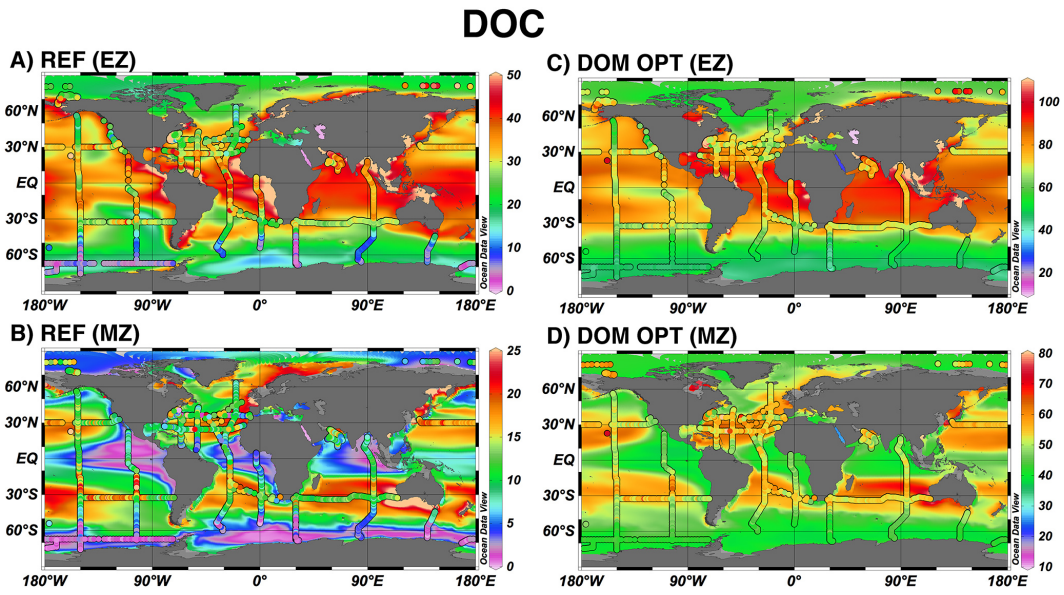

Figure 3. Plots of simulated semilabile [DOC] (μM; colored contours) with observations (colored dots) for the REF simulation at **(a)** the surface (EZ) and **(b)** 200 m (MZ). Total [DOC] (μM; semilabile + refractory) for the DOM OPT simulation is shown for **(c)** the surface (EZ) and **(d)** 200 m (MZ). Note the difference in color scales between plots **(a)** and **(c)**; **(b)** and **(d)** as the REF simulation lacks a DOCr tracer.

DON. Total euphotic zone DON production is 120 Tmol N yr^{-1} with a >100 m depth export of 25.0 Tmol N yr^{-1} (Table 2). Modeled total DON concentrations (semilabile + refractory) at the surface are similarly overestimated in the REF simulation (Table 3) by up to 100 % within the subtropical gyres of the Pacific and the eastern South Atlantic oceans (Fig. 4a). Model–observation misfit is better at 200 m (Fig. 4b); however, biases of 15–25 % remain (Table 3) in a number of regions (e.g., central equatorial Pacific and southern Indian oceans).

DOP. Total euphotic zone DOP production is 7.43 Tmol P yr^{-1} with export out of the euphotic zone valued at 1.30 Tmol P yr^{-1} (Table 2). Modeled DOP distributions are shown in Fig. 5a (surface), and 5b (200 m), with observations mostly limited to the Atlantic Ocean. The region of elevated simulated DOP (> 0.25 μM) in the eastern South Atlantic surface waters is located further to the east than is observed (Fig. 5a), possibly owing to the snapshot nature of the observations (collected in January–February) compared to the annually averaged simulation. Modeled DOP in the subsurface agrees reasonably well with the Atlantic observations, except for a ∼ 70 % model overestimate in the South Atlantic subtropical gyre (Fig. 5b).

3.3 Modeled DOM in the DOM OPT simulation

Results and comparison of DOM cycling metrics from the DOM OPT simulation against the observational data set and REF simulation are presented in Tables 2 and 3. For a comparison of the set of DOM cycling parameter values between the REF and DOM OPT simulations, see Table 1.

DOC. Total DOC production in the euphotic zone (upper 100 m) for the DOM OPT simulation is 4.16 Pg C yr^{-1} (Table 2). About 45 % of this DOC is remineralized within the euphotic zone, yielding DOC export from the EZ of 2.28 Pg C yr^{-1}, which is ∼ 20 % larger than the result from a separate DOC data assimilative modeling study (Table 2; Hansell et al., 2009). Combined with the particulate organic carbon export from 100 m in the DOM OPT simulation of 7.01 Pg C yr^{-1}, DOC contributes ∼ 25 % to the total 9.29 Pg C yr^{-1} of export production in the CESM BEC. Modeled total DOC concentrations (semilabile + refractory) from the DOM OPT simulation are shown for the surface (Fig. 3c) and at 200 m (Fig. 3d). There is generally good agreement between the simulated fields and observations (colored dots) with the mean bias being < 20 % for the upper ocean (0–500 m; Table 3). Slightly larger model overestimations (up to ∼ 30 %) exist at the surface for certain low-latitude ocean basins (e.g., tropical Atlantic, and Indian oceans).

DON. Total euphotic zone DON production is 30.7 Tmol N yr^{-1} with a >100 m depth export of 16.4 Tmol N yr^{-1} (Table 2). Modeled total DON concentrations are improved over the REF simulation at 200 m (Fig. 4d); however, overestimations of DON at the surface remain in DOM OPT (Fig. 4c). Simulated surface DON overestimation is largest in the low to mid latitudes, reaching ∼ 30 %. Opposite the pattern obtained for the low latitudes, high-latitude simulated DON is underestimated at the surface in the Southern Ocean (Fig. 4c) by up to ∼ 35 %. However, overall, DON mean biases are small in the DOM OPT simulation, i.e., < 10 % (Table 3).

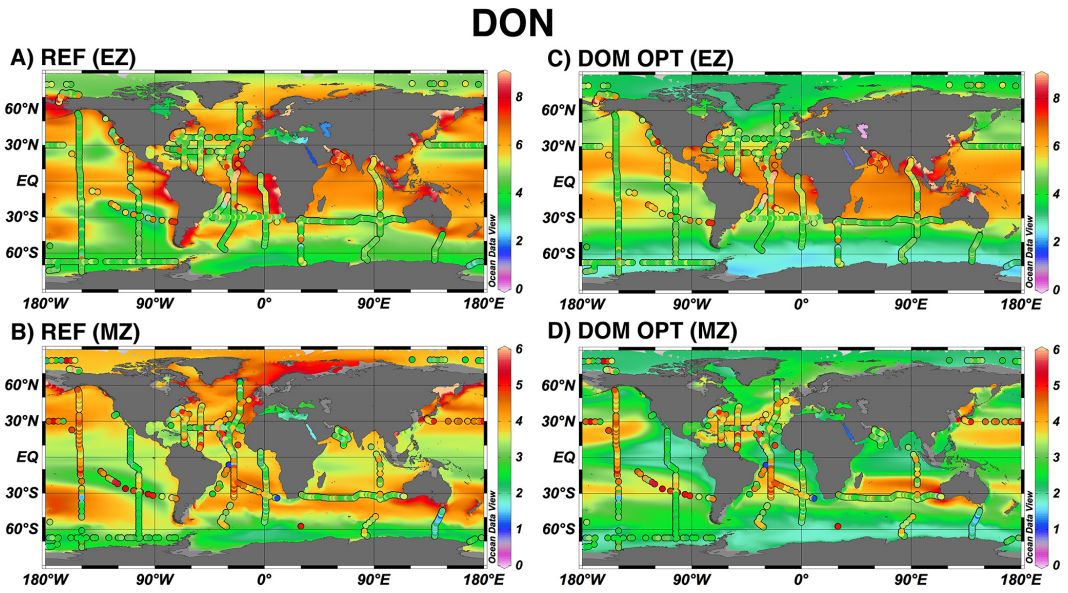

Figure 4. Plots of simulated total [DON] (µM; colored contours) with observations (colored dots) for the REF simulation at **(a)** the surface (EZ) and **(b)** 200 m (MZ), and for the DOM OPT simulation at **(c)** the surface (EZ) and **(d)** 200 m (MZ).

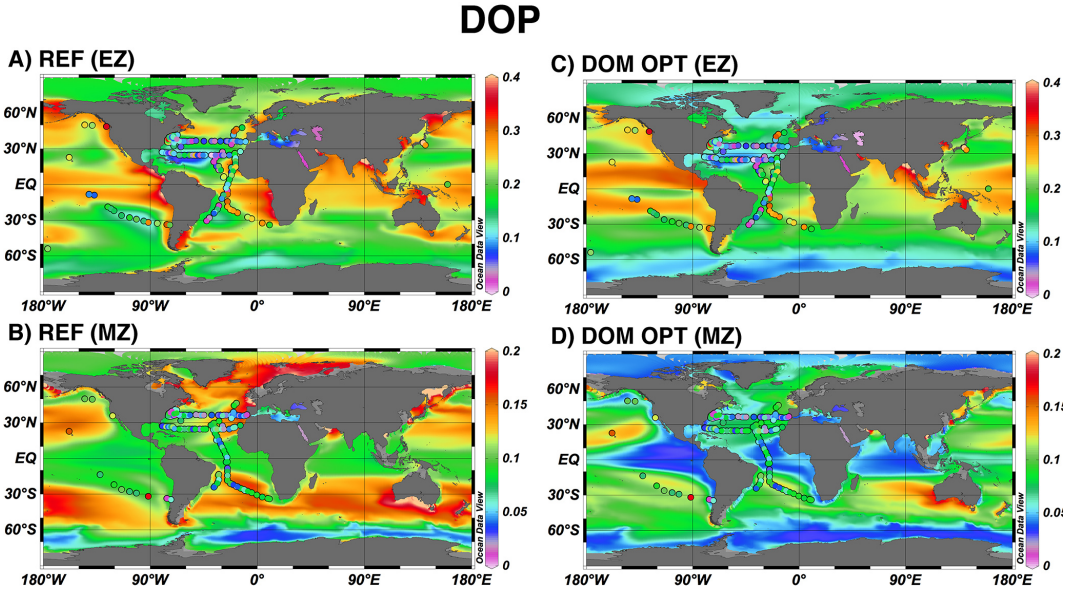

Figure 5. Plots of simulated total [DOP] (µM; colored contours) with observations (colored dots) for the REF simulation at **(a)** the surface (EZ) and **(b)** 200 m (MZ), and for the DOM OPT simulation at **(c)** the surface (EZ) and **(d)** 200 m (MZ).

DOP. Total euphotic zone DOP production is 2.94 Tmol P yr^{-1} with export out of the euphotic zone of ∼1 Tmol P yr^{-1} (Table 2). Modeled DOP distributions are shown in Fig. 5c (surface), and 5d (200 m). The DOM OPT simulation captures the low DOP concentrations observed in the North Atlantic, largely due to enhanced phytoplankton direct uptake of DOP (see Sect. 3.5). The region of elevated simulated DOP (> 0.25 µM) in the eastern South Atlantic surface waters continues to be located further to the east than is observed (Fig. 5c) in the DOM OPT simulation as was also the case in the REF simulation. Modeled DOP in the subsurface agrees reasonably well with the Atlantic observations, reducing the large overestimates in the REF simulation (Fig. 5d, b). Overall, mean DOP biases are similarly < 10 % for both the total and semilabile pools (Table 3).

Table 4. DOM mean bias and correlation coefficient in relation to the DOM observations within the upper ocean (0–500 m depth) for the REF, DOM OPT, REDFIELD, and EZRAPID ∼ 3° simulations. Observations of semilabile DOM are calculated as the total observed DOM concentration less the asymptotic concentration below 1000 m in each ocean basin.

Metric	REF		DOM OPT		REDFIELD		EZRAPID	
Total DOM 0–500 m	mean bias	log r	mean bias	log r	mean bias	log r	mean bias	log r
DOC	NA	NA	+3 %	0.772	−1 %	0.752	+15 %	0.764
DON	+6 %	0.556	0 %	0.622	+24 %	0.609	+16 %	0.601
DOP	+13 %	0.394	−16 %	0.383	+121 %	0.440	+7 %	0.300
Semilabile DOM 0–500 m								
DOC	+3 %	0.770	+30 %	0.800	+18 %	0.784	+71 %	0.799
DON	−33 %	0.648	−4 %	0.617	+36 %	0.605	+25%	0.609
DOP	−10 %	0.418	−25 %	0.380	+136 %	0.441	+5 %	0.298

3.4 Comparison of multiple DOM cycling schemes in the CESM BEC

We have also tested other hypotheses for DOM cycling formulations such as non-variable C : N : P cycling stoichiometry (i.e., DOM cycling occurs at the Redfield ratio) as well as more rapid turnover of DOM in the EZ compared to the MZ (the DOM OPT simulation contains more rapid turnover of DOM in the MZ, following the work of Carlson et al., 2004; Letscher et al., 2013a). To test these hypotheses, we performed two additional BEC simulations termed REDFIELD and EZRAPID using a coarser-resolution version of the BEC model with a nominal 3° horizontal resolution. The optimized cycling parameter values obtained for DOC from the DOM OPT simulation were assigned to the DON and DOP pools for the REDFIELD simulation to allow all DOM (C : N : P) to cycle at the same rate and in the same proportions. The ability for phytoplankton to directly utilize DOP is also turned off in the REDFIELD simulation. The optimized EZ and MZ lifetimes for each DOM tracer from the DOM OPT simulation were reversed for the EZRAPID simulation such that the shorter lifetime (more rapid remineralization rate) was assigned to SLDOM in the EZ.

Results from 310 yr simulations of these are compared against ∼ 3° simulations of REF and DOM OPT in Table 4. Results are similar for DOC when comparing the DOM OPT and REDFIELD simulations, which is to be expected as the REDFIELD simulation used the same DOC cycling parameters as the DOM OPT simulation. Faster turnover of DOC in the EZ (EZRAPID simulations) had a detrimental effect on DOC mean biases, resulting in large overestimations in the upper 500 m (Table 4) when compared with faster turnover in the MZ (DOM OPT). Large positive mean biases were also found for DON within the REDFIELD and EZRAPID simulations when compared to the DOM OPT (Table 4). Similar positive biases were found for DOP within the REDFIELD and especially for the EZRAPID simulations, i.e., up to ∼ 135 % (Table 4).

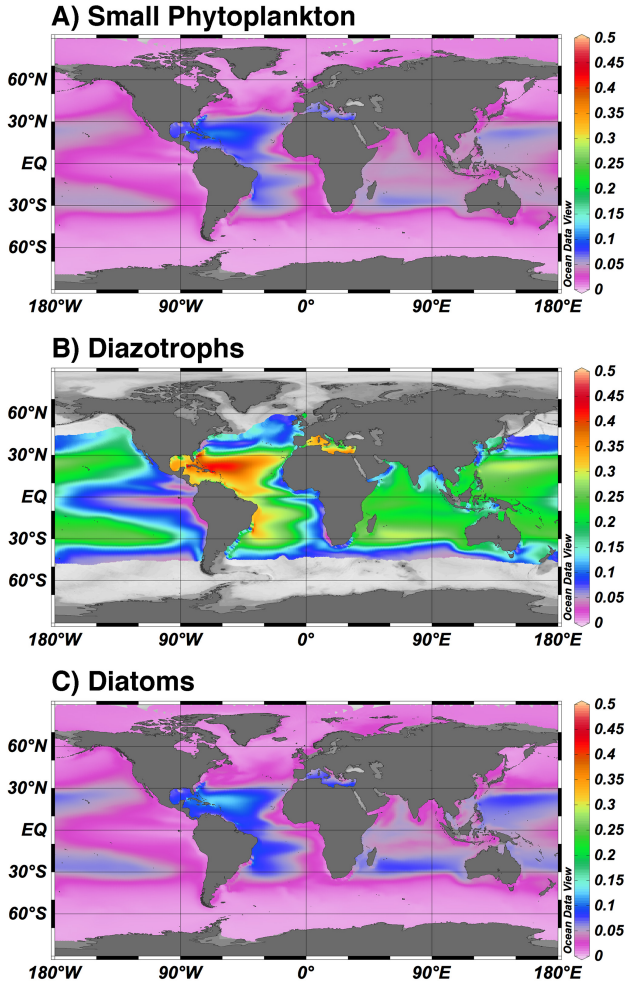

Figure 6. Fraction of total P uptake from DOP integrated over the euphotic zone (upper 100 m) for **(a)** small phytoplankton, **(b)** diazotrophs, and **(c)** diatoms in the DOM OPT simulation.

3.5 Direct DOP uptake by phytoplankton

The longer lifetimes for semilabile DOP in the DOM OPT simulation (on the order of years) allow for significant horizontal advection of DOP from the more productive gyre margins (e.g., the NW African upwelling region) towards the Sargasso Sea, providing an additional phosphorus source to the western North Atlantic. Each phytoplankton group within the BEC model can directly utilize DOP to satisfy their phosphorus requirements when phosphate concentrations are low (Moore et al., 2014). Literature reports of this phenomenon are numerous (e.g., Bjorkman and Karl, 2003; Casey et al., 2009; Lomas et al., 2010; Orchard et al., 2010) whereby phytoplankton make use of extracellular alkaline phosphatases to cleave phosphate groups from DOP moieties such as phosphate mono- and diesters (Dyhrman and Ruttenberg, 2006; Sato et al., 2013) for subsequent uptake of the liberated phosphorus. Sohm and Capone (2006) provide half-saturation constants for DOP uptake by *Trichodesmium* spp. (a diazotroph) and bulk phytoplankton (dominated by nano- and picophytoplankton) from the subtropical North Atlantic, and suggested *Trichodesmium* species obtained much of their required phosphorus from DOP in this region. Based partly on this study, the diazotrophs have been given a lower half-saturation constant for DOP uptake than the other phytoplankton (Moore et al., 2014). Diatoms also exhibit alkaline phosphatase activity albeit at lower rates than other plankton groups (Dyhrman and Ruttenberg, 2006; Nicholson et al., 2006), and were thus assigned a greater half-saturation for DOP uptake than the other phytoplankton groups in the BEC (consistent with their reduced efficiency in taking up dissolved inorganic phosphorus in the model).

The fraction of total phosphorus uptake that is sustained by DOP uptake for each phytoplankton group in the DOM OPT simulation is shown in Fig. 6. DOP uptake is largest by diazotrophs (Fig. 6b), with generally $\sim 20\,\%$ of P uptake from DOP in the subtropical gyres, increasing to ~ 30–$50\,\%$ in the subtropical North Atlantic, western side of the subtropical South Atlantic, and the eastern Mediterranean Sea. DOP uptake represents a small fraction ($< 5\,\%$) of P uptake by the small phytoplankton and diatoms (Fig. 6a, c) over much of the ocean, increasing to $\sim 10\,\%$ in the subtropical ocean gyres.

4 Discussion and summary

This study utilized a rapid solver of a simple linear biogeochemical cycling ocean model, constrained by our compilation of marine DOM observations, to efficiently optimize DOM biogeochemistry in the larger complexity CESM BEC model. This approach allows for a quicker and more quantitatively robust method for optimizing biogeochemical ocean model parameters over the traditional "hand"-tuning approach. Model parameters determined with the modified DMI-enabled linear DOM model carried over well when implemented in the full CESM BEC (see Fig. 2). The DOM OPT simulation contains reduced mean biases, improved correlation coefficients, and is more consistent with the DOM observational constraints when compared to the REF simulation (Figs. 3, 4, 5; Tables 2, 3).

Our results demonstrate that allowing for non-Redfield stoichiometry in the DOM pools significantly improves the match to observed DOM distributions. The order of lability follows P > N > C, diagnosed from the calculated effective tracer lifetimes in DOM OPT which include the net result of the sum of tracer sinks (~ 3.2 vs. 6.3 vs. 6.8 yr for semilabile P, N, C; ~ 4300 vs. 6360 vs. 13 900 yr for refractory P, N, and C). The exact values of the DOM lifetimes determined in our study are dependent on the underlying ocean circulation model used; however, Hansell et al. (2012) determined similar values for refractory DOC (16 000 yr) and combined semilabile and semirefractory DOC (~ 7 yr; estimated from their Fig. 5) while using a distinct ocean circulation model than the one employed in the current study. In addition, the DOM lifetimes from the DOM OPT simulation are in general agreement with available estimates from the literature. Semilabile DOC lifetime has been estimated at ~ 1–13 yr in the mesopelagic zone of the Sargasso Sea (Hansell and Carlson, 2001), and ~ 7–22 yr in the mesopelagic zone of the North Pacific subtropical gyre (Abell et al., 2000). Semilabile DON lifetimes have been estimated at ~ 3–12 yr (Letscher et al., 2013a) or ~ 11–20 yr (Abell et al., 2000) for marine DON and ~ 4–14 yr for terrigenous-derived DON in the Arctic Ocean (Letscher et al., 2013b).

Our DOM OPT simulation-estimated export C : N : P ratio of 225 : 19 : 1 for the semilabile DOM is in excellent agreement with the estimate of 199 : 20 : 1 by Hopkinson and Vallino (2005) and strongly supports the idea that DOC is exported efficiently relative to DOP compared with the canonical Redfield ratio. The calculated export efficiencies, that is the fraction of euphotic zone DOM production that is exported below 100 m, are 55, 53, and 17.5 % for DOC, DON, and DOP, respectively.

We found that best agreement with observed DOM distributions required a more rapid degradation of semilabile DOM in the mesopelagic than in the euphotic zone. This result is consistent with some incubation studies of DOM degradation (Carlson et al., 2004; Letscher et al., 2013a). Possible hypotheses for this depth dependence on DOM lifetimes in the real ocean are numerous, including differences in DOM composition/quality (Skoog and Benner, 1997; Aluwihare et al., 2005; Goldberg et al., 2011), microbial community structure (Giovannoni et al., 1996; Delong et al., 2006; Treusch et al., 2009; Carlson et al., 2004, 2009; Morris et al., 2012), availability of inorganic nutrients for heterotrophic utilization (Cotner et al., 1997; Rivkin and Anderson, 1997; Caron et al., 2000), abundance of bacterial grazers (Caron et al., 2000), and the presence or specific affinity of microbial cell membrane nutrient transporters (Azam and Malfatti,

2007; Morris et al., 2010). However, the relative importance of each of these mechanisms is not well constrained, nor are any considered in the BEC model formulation, and thus require further investigation.

Direct uptake of DOP by phytoplankton seemed necessary in our simulations to capture the observed very low surface DOP concentrations in the Sargasso Sea. Yet there are large uncertainties in the preference and uptake efficiencies for dissolved inorganic phosphorus versus dissolved organic phosphorus by different phytoplankton groups. Future field and lab studies are needed to reduce these uncertainties and to better quantify the role of DOP in determining spatial patterns of nitrogen fixation. There is also a great need for additional DOP measurements in every basin except the North Atlantic, along with improved quality control and the development of a DOP standard reference material.

Acknowledgements. The authors thank Ann Bardin and Keith Lindsay for their contribution to the development of the CESM POP2 offline transport matrix that was used for the DMI solver. We would also like to thank the British Oceanographic Data Centre and all of the principal investigators involved with production and sharing of DOM data from the Atlantic including Claire Mahaffey, Sinhue Torres-Valdés, Xi Pan, Malcolm Woodward, Rhiannon Mather, Angela Landolfi, and Richard Sanders. This work was supported by grant ER65358 from the U.S. Department of Energy Office of Biological and Environmental Research to F. Primeau and J. K. Moore. J. K. Moore also acknowledges support from the National Science Foundation grants AGS-1021776 and AGS-1048890.

Edited by: K. Thonicke

References

Abell, J., Emerson, S., and Renaud, P.: Distributions of TOP, TON, and TOC in the North Pacific subtropical gyre: Implications for nutrient supply in the surface ocean and remineralization in the upper thermocline, J. Mar. Res., 58, 203–222, 2000.

Aluwihare, L. I., Repeta, D. J., Pantoja, S., and Johnson, C. G.: Two chemically distinct pools of organic nitrogen accumulate in the ocean, Science, 308, 1007–1010, 2005.

Amestoy, P. R., Duff, I. S., Koster, J., and L'Excellent, J.-Y.: A fully asynchronous multifrontal solver using distributed dynamic scheduling, SIAM Journal of Matrix Analysis and Applications, 23, 15–41, 2001.

Amestoy, P. R., Guermouche, A., L'Excellent, J.-Y., and Pralet, S.: Hybrid scheduling for the parallel solution of linear systems, Parallel Computing, 32, 136–156, 2006.

Aminot, A. and Kérouel, R.: Dissolved organic carbon, nitrogen and phosphorus in the NE Atlantic and the NW Mediterranean with particular reference to non-refractory fractions and degradation, Deep Sea Res. I, 51, 1975–1999, 2004.

Anderson, L. A. and Sarmiento, J. L.: Redfield ratios of remineralization determined by nutrient data analysis, Global Biogeochem. Cy., 8, 65–80, 1994.

Azam, F. and Malfatti, F.: Microbial structuring of marine ecosystems, Nature Rev. Microbiol., 5, 782–791, 2007.

Bardin, A., Primeau, F., and Lindsay, K.: An offline implicit solver for simulating prebomb radiocarbon, Ocean Model., 73, 45–58, 2014.

Bjorkman, K. M. and Karl, D. M.: Bioavailability of dissolved organic phosphorus in the euphotic zone at Station ALOHA, North Pacific Subtropical Gyre, Limnol. Oceanogr., 48, 1049–1057, 2003.

Carlson, C. A.: Production and removal processes, in: Biogeochemistry of marine dissolved organic matter, edited by: Hansell, D. A. and Carlson, C. A., Academic Press, San Diego, 91–151, 2002.

Carlson, C. A., Giovannoni, S. J., Hansell, D. A., Goldberg, S. J., Parsons, R., and Vergin, K.: Interactions between DOC, microbial processes, and community structure in the mesopelagic zone of the northwestern Sargasso Sea, Limnol. Oceanogr., 49, 1073–1083, 2004.

Carlson, C. A., Morris, R., Parsons, R., Treusch, A. H., Giovannoni, S. J., and Vergin, K. (2008): Seasonal dynamics of SAR11 populations in the euphotic and mesopelagic zones of the northwestern Sargasso Sea, The ISME Journal, 3, 283–295, 2009.

Caron, D. A., Lim, E. L., Sanders, R. W., Dennett, M. R., and Berninger, U. G.: Responses of bacterioplankton and phytoplankton to organic carbon and inorganic nutrient additions in contrasting oceanic ecosystems, Aquat. Microbial. Ecol., 22, 175–184, 2000.

Casey, J. R., Lomas, M. W., Michelou, V. K., Dyhrman, S. T., Orchard, E. D., Ammerman, J. W., and Sylvan, J. B.: Phytoplankton taxon-specific orthophosphate (Pi) and ATP utilization in the western subtropical North Atlantic, Aquat. Microbial. Ecol., 58, 31, 31–44, 2009.

Cotner, J. B., Ammerman, J. W., Peele, E. R., and Bentzen, E.: Phosphorus-limited bacterioplankton growth in the Sargasso Sea, Aquat. Microbial. Ecol., 13, 141–149, 1997.

Danabasoglu, G., Bates, S. C., Briegleb, B. P., Jayne, S. R., Jochum, M., Large, W. G., and Yeager, S. G.: The CCSM4 ocean component, J. Climate, 25, 1361–1389, 2011.

DeLong, E. F., Preston, C. M., Mincer, T., Rich, V., Hallam, S. J., Frigaard, N. U., and Karl, D. M.: Community genomics among stratified microbial assemblages in the ocean's interior, Science, 311, 496–503, 2006.

Dunne, J. P., John, J. G., Shevliakova, E., Stouffer, R. J., Krasting, J. P., Malyshev, S. L., Milly, P. C. D., Sentman, L. T., Adcroft, A. J., Cooke, W., Dunne, K. A., Griffies, S. M., Hallberg, R. W., Harrison, M. J., Levy, H., Wittenberg, A. T., Phillips, P. J., and Zadeh, N.: GFDL's ESM2 global coupled climate-carbon Earth System Models Part II: Carbon system formulation and baseline simulation characteristics, J. Climate, 26, 2247–2267, 2013.

Dyhrman, S. T. and Ruttenberg, K. C.: Presence and regulation of alkaline phosphatase activity in eukaryotic phytoplankton from the coastal ocean: Implications for dissolved organic phosphorus remineralization, Limnol. Oceanogr., 51, 1381–1390, 2006.

Gent, P. R., Danabasoglu, G., Donner, L. J., Holland, M. M., Hunke, E. C., Jayne, S. R., and Zhang, M.: The community climate system model version 4, J. Climate, 24, 4973–4991, 2011.

Giovannoni, S. J., Rappé, M. S., Vergin, K. L., and Adair, N. L.: 16S rRNA genes reveal stratified open ocean bacterioplankton popu-

lations related to the green non-sulfur bacteria, P. Natl. Acad. Sci., 93, 7979–7984, 1996.

Goldberg, S. J., Carlson, C. A., Brzezinski, M., Nelson, N. B., and Siegel, D. A.: Systematic removal of neutral sugars within dissolved organic matter across ocean basins, Geophys. Res. Lett., 38, L17606, doi:10.1029/2011GL048620, 2011.

Hansell, D. A.: Recalcitrant dissolved organic carbon fractions, Ann. Rev. Mar. Sci., 5, 421–445, 2013.

Hansell, D. A. and Carlson, C. A.: Biogeochemistry of total organic carbon and nitrogen in the Sargasso Sea: control by convective overturn, Deep Sea Res. II, 48, 1649–1667, 2001.

Hansell, D. A., Carlson, C. A., Repeta, D. J., and Schlitzer, R.: Dissolved organic matter in the ocean: A controversy stimulates new insights, Oceanography, 22, 202–211, 2009.

Hansell, D. A., Carlson, C. A., and Schlitzer, R.: Net removal of major marine dissolved organic carbon fractions in the subsurface ocean, Global Biogeochem. Cy., 26, GB1016, doi:10.1029/2011GB004069, 2012.

Hopkinson, C. S. and Vallino, J. J.: Efficient export of carbon to the deep ocean through dissolved organic matter, Nature, 433, 142–145, 2005.

Khatiwala, S., Visbeck, M., and Cane, M. A.: Accelerated simulation of passive tracers in ocean circulation models, Ocean Modell., 9, 51–69, 2005.

Kim, J. M., Lee, K., Shin, K., Yang, E. J., Engel, A., Karl, D. M., and Kim, H. C.: Shifts in biogenic carbon flow from particulate to dissolved forms under high carbon dioxide and warm ocean conditions, Geophys. Res. Lett., 38, L08612, doi:10.1029/2011GL047346, 2011.

Kwon, E. Y. and Primeau, F.: Optimization and sensitivity study of a biogeochemistry model using an implicit solver and in situ phosphate data, Global Biogeochem. Cy., 20, GB4009, doi:10.1029/2005GB002631, 2006.

Letscher, R. T. and Moore, J. K.: Preferential remineralization of dissolved organic phosphorus and non-Redfield DOM dynamics in the global ocean, Global Biogeochem. Cy., under review, 2014.

Letscher, R. T., Hansell, D. A., Carlson, C. A., Lumpkin, R., and Knapp, A. N.: Dissolved organic nitrogen in the global surface ocean: Distribution and fate, Global Biogeochem. Cy., 27, 141–153, 2013a.

Letscher, R. T., Hansell, D. A., Kadko, D., and Bates, N. R.: Dissolved organic nitrogen dynamics in the Arctic Ocean, Mar. Chem., 148, 1–9, 2013b.

Lomas, M. W., Burke, A. L., Lomas, D. A., Bell, D. W., Shen, C., Dyhrman, S. T., and Ammerman, J. W.: Sargasso Sea phosphorus biogeochemistry: an important role for dissolved organic phosphorus (DOP), Biogeosciences, 7, 695–710, doi:10.5194/bg-7-695-2010, 2010.

Martiny, A. C., Pham, C. T. A., Primeau, F. W., Vrugt, J. A., Moore, J. K., Levin, S. A., and Lomas, M. W.: Strong latitudinal patterns in the elemental ratios of marine plankton and organic matter, Nature Geosci., 6, 279–283, 2013a.

Martiny, A. C., Vrugt, J. A., Primeau, F. W., and Lomas, M. W.: Regional variation in the particulate organic carbon to nitrogen ratio in the surface ocean, Global Biogeochem. Cy., 27, 723–731, 2013b.

Moore, J. K., Doney, S. C., and Lindsay, K.: Upper ocean ecosystem dynamics and iron cycling in a global three-dimensional model, Global Biogeochem. Cy., 18, GB4028, doi:10.1029/2004GB002220, 2004.

Moore, J. K., Lindsay, K., Doney, S. C., Long, M. C., and Misumi, K.: Ecosystem Dynamics and biogeochemical cycling in the Community Earth System Model [CESM1(BGC)]: Comparison of the 1990s with the 2090s under the RCP4.5 and RCP8.5 Scenarios, J. Climate, 26, 9291–9312, 2013.

Moore, J. K., Lindsay, K., Letscher, R. T., and Mayorga, E.: Improving ocean biogeochemistry simulation in the Community Earth System Model, Geosci. Model Dev. Discuss., in preparation, 2014.

Morris, R. M., Nunn, B. L., Frazar, C., Goodlett, D. R., Ting, Y. S., and Rocap, G.: Comparative metaproteomics reveals ocean-scale shifts in microbial nutrient utilization and energy transduction, The ISME Journal, 4, 673–685, 2010.

Morris, R. M., Frazar, C. D., and Carlson, C. A.: Basin-scale patterns in the abundance of SAR11 subclades, marine Actinobacteria (OM1), members of the Roseobacter clade and OCS116 in the South Atlantic, Environ. Microbiol., 14, 1133–1144, 2012.

Nicholson, D., Dyhrman, S., Chavez, F., and Paytan, A.: Alkaline phosphatase activity in the phytoplankton communities of Monterey Bay and San Francisco Bay, Limnol. Oceanogr., 51, 874–883, 2006.

Orchard, E. D., Ammerman, J. W., Lomas, M. W., and Dyhrman, S. T.: Dissolved inorganic and organic phosphorus uptake in Trichodesmium and the microbial community: The importance of phosphorus ester in the Sargasso Sea, Limnol. Oceanogr., 55, 1390–1399, 2010.

Redfield, A. C.: The biological control of chemical factors in the environment, American Scientist, 46, 205–221, 1958.

Redfield, A. C., Ketchum, B. H., and Richards, F. A.: The influence of organisms on the composition of seawater, in: The sea: ideas and observations on progress in the study of the seas, Wiley, 2, 1963.

Rivkin, R. B. and Anderson, M. R.: Inorganic nutrient limitation of oceanic bacterioplankton, Limnol. Oceanogr., 730–740, 1997.

Sato, M., Sakuraba, R., and Hashihama, F.: Phosphate monoesterase and diesterase activities in the North and South Pacific Ocean, Biogeosciences, 10, 7677–7688, doi:10.5194/bg-10-7677-2013, 2013.

Skoog, A. and Benner, R.: Aldoses in various size fractions of marine organic matter: Implications for carbon cycling, Limnol. Oceanogr., 42, 1803–1813, 1997.

Smith, R. D., Jones, P. W., Briegleb, B., Bryan, F., Danabasoglu, G., Dennis, J., and Yeager, S.: The parallel ocean program (POP) reference manual: ocean component of the community climate system model (CCSM), Los Alamos National Laboratory, LAUR-10-01853, 2010.

Sohm, J. A. and Capone, D. G.: Phosphorus dynamics of the tropical and subtropical north Atlantic: Trichodesmium spp. versus bulk plankton, Mar. Ecol. Prog. Ser., 317, 21, 21–28, 2006.

Treusch, A. H., Vergin, K. L., Finlay, L. A., Donatz, M. G., Burton, R. M., Carlson, C. A., and Giovannoni, S. J.: Seasonality and vertical structure of microbial communities in an ocean gyre, The ISME Journal, 3, 1148–1163, 2009.

Vichi, M., Pinardi, N., and Masina, S.: A generalized model of pelagic biogeochemistry for the global ocean ecosystem, Part I: Theory, J. Mar. Syst., 64, 89–109, 2007.

Wohlers, J., Engel, A., Zöllner, E., Breithaupt, P., Jürgens, K., Hoppe, H. G., and Riebesell, U.: Changes in biogenic carbon flow in response to sea surface warming, P. Natl. Acad. Sci., 106, 7067–7072, 2009.